Numerical study of 1+1D, moment-based drift kinetic models with periodic boundary conditions

M. Barnes[1], **F. I. Parra**[1], **M. R. Hardman**[1] **and J. Omotani**[2]

[1] Rudolf Peierls Centre for Theoretical Physics, University of Oxford, Clarendon Laboratory, Parks Road, Oxford OX1 3PU, United Kingdom
[2] Culham Centre for Fusion Energy, Culham Science Centre, Abingdon, Oxon, OX14 3DB, United Kingdom

E-mail: `michael.barnes@physics.ox.ac.uk`

1. Introduction

We expect that one of the biggest challenges in numerically solving drift kinetic equations in the plasma edge is treating the motion of electrons along the magnetic field. Because the electrons are light, they move rapidly along the field, placing a severe stability restriction on the step size for explicit time advance schemes. Unfortunately, an implicit treatment is not straightforward due to an implicit dependence of the electrostatic potential on the charged particle distribution functions. One of the main aims of our research is to develop and test a novel analytical model and associated numerical algorithm for relaxing this restriction. As a first step towards this goal, we developed a new code in the programming language Julia to simulate a simple model for parallel dynamics (described in our Feb 2021 report [1]) without the novel moment-based approach that we intend to explore. We have now extended the code to simulate a modified set of equations in which the density is removed from the particle distribution function and is evolved separately using the continuity equation. In this report we give an overview of this moment-based approach and discuss the numerical issues around its implementation.

2. Model equations

A detailed derivation of the model we consider is provided in our Jan 2021 report [2]. Here we reproduce a brief overview of the model from our Feb 2021 report [1] for the Reader's convenience. The model we consider consists of a single ion species of charge e, a single neutral species, and an electron species modelled as having a Boltzmann response, all immersed in a straight, uniform magnetic field in the z direction. We allow for charge exchange collisions between ions and neutrals but do not account for intra-species collisions. Finally, we assume that the plasma is homogeneous in the plane perpendicular to the magnetic field. With these assumptions, our model system of

1

equations is

$$\frac{\partial f_i}{\partial t} + v_\parallel \frac{\partial f_i}{\partial z} - \frac{e}{m_i} \frac{\partial \phi}{\partial z} \frac{\partial f_i}{\partial v_\parallel} = -R_{in} \left(n_n f_i - n_i f_n \right), \tag{1}$$

$$\frac{\partial f_n}{\partial t} + v_\parallel \frac{\partial f_n}{\partial z} = -R_{in} \left(n_i f_n - n_n f_i \right), \tag{2}$$

$$n_s(z,t) = \int_{-\infty}^{\infty} dv_\parallel f_s(z, v_\parallel, t), \tag{3}$$

and

$$n_i = N_e \exp\left(\frac{e\phi}{T_e} \right), \tag{4}$$

with $f_s \doteq \int d\vartheta dv_\perp v_\perp F_s$ the marginalized particle distribution function for species s, $v_\parallel$ and $v_\perp$ the components of the particle velocity parallel and perpendicular to the magnetic field, respectively, ϑ the gyro-angle, m_i the ion mass, t the time, ϕ the electrostatic potential, and R_{in} the charge exchange collision frequency.

For our boundary conditions, we impose periodicity on f_s in both z and $v_\parallel$, with periods L_z and $L_{v_\parallel}$, respectively. There is also the option to impose zero boundary conditions on z and $v_\parallel$ at the upwind boundary of the domain. As f_s should go to zero at $v_\parallel \to \pm\infty$, imposition of zero boundary conditions and periodic boundary conditions should be equivalent as long as $L_{v_\parallel}$ is sufficiently large. Note that with either choice of boundary conditions, the line-averaged density $\int_0^{L_z} dz\, n_s$ is conserved.

We normalize Eqs. (1)-(4) by defining

$$\tilde{f}_s \doteq f_s \frac{v_{\text{th,i}} \sqrt{\pi}}{N_e}, \tag{5}$$

$$\tilde{t} \doteq t \frac{v_{\text{th,i}}}{L_z}, \tag{6}$$

$$\tilde{z} \doteq \frac{z}{L_z}, \tag{7}$$

$$\tilde{v}_\parallel \doteq \frac{v_\parallel}{v_{\text{th,i}}}, \tag{8}$$

$$\tilde{n}_s \doteq \frac{n_s}{N_e}, \tag{9}$$

$$\tilde{\phi} \doteq \frac{e\phi}{T_e}, \tag{10}$$

and

$$\tilde{R}_{\text{in}} \doteq R_{\text{in}} \frac{N_e L_z}{v_{\text{th,i}}} \tag{11}$$

with $v_{\text{th,i}} \doteq \sqrt{2T_e/m_i}$. In terms of these normalised quantities, Eqs (1)-(4) become

$$\frac{\partial \tilde{f}_i}{\partial \tilde{t}} + \tilde{v}_\parallel \frac{\partial \tilde{f}_i}{\partial \tilde{z}} - \frac{1}{2} \frac{\partial \tilde{\phi}}{\partial \tilde{z}} \frac{\partial \tilde{f}_i}{\partial \tilde{v}_\parallel} = -\tilde{R}_{\text{in}} \left(\tilde{n}_n \tilde{f}_i - \tilde{n}_i \tilde{f}_n \right), \tag{12}$$

$$\frac{\partial \tilde{f}_n}{\partial \tilde{t}} + \tilde{v}_\parallel \frac{\partial \tilde{f}_n}{\partial \tilde{z}} = -\tilde{R}_{\text{in}} \left(\tilde{n}_i \tilde{f}_n - \tilde{n}_n \tilde{f}_i \right), \tag{13}$$

$$e^{\tilde{\phi}} = \tilde{n}_i = \frac{1}{\sqrt{\pi}} \int_{-\infty}^{\infty} d\tilde{v}_\parallel \tilde{f}_i, \tag{14}$$

and

$$\tilde{n}_n = \frac{1}{\sqrt{\pi}} \int_{-\infty}^{\infty} d\tilde{v}_\parallel \tilde{f}_n. \tag{15}$$

2.1. Moment approach: density

We now define the modified distribution function $g_s \doteq f_s/n_s$ so that $\int dv_\parallel g_s = 1$. In terms of g_s, the system of equations given by Eqs. (1)-(4) becomes

$$n_i \left(\frac{\partial g_i}{\partial t} + v_\parallel \frac{\partial g_i}{\partial z} - \frac{e}{m_i} \frac{\partial \phi}{\partial z} \frac{\partial g_i}{\partial v_\parallel} \right) + g_i \left(\frac{\partial n_i}{\partial t} + v_\parallel \frac{\partial n_i}{\partial z} \right) = -R_{\text{in}} n_i n_n \left(g_i - g_n \right), \tag{16}$$

$$n_n \left(\frac{\partial g_n}{\partial t} + v_\parallel \frac{\partial g_n}{\partial z} \right) + g_n \left(\frac{\partial n_n}{\partial t} + v_\parallel \frac{\partial n_n}{\partial z} \right) = -R_{\text{in}} n_i n_n \left(g_n - g_i \right), \tag{17}$$

$$n_i = N_e \exp \left(\frac{e\phi}{T_e} \right), \tag{18}$$

$$\frac{\partial n_s}{\partial t} + \frac{\partial n_s u_s}{\partial z} = 0, \tag{19}$$

and

$$u_s = \int_{-\infty}^{\infty} dv_\parallel g_s v_\parallel. \tag{20}$$

Note that the 1D continuity equation (19) has replaced the moment equation (3) as a means of computing the density for each species.

Substituting the continuity equation (19) into the drift kinetic equations (16) and (17) gives

$$\frac{\partial g_i}{\partial t} + v_\parallel \frac{\partial g_i}{\partial z} - \frac{e}{m_i} \frac{\partial \phi}{\partial z} \frac{\partial g_i}{\partial v_\parallel} = -R_{\text{in}} n_n \left(g_i - g_n \right) + g_i \left(\frac{\partial u_i}{\partial z} - \left(v_\parallel - u_i \right) \frac{\partial \ln n_i}{\partial z} \right) \tag{21}$$

and

$$\frac{\partial g_n}{\partial t} + v_\parallel \frac{\partial g_n}{\partial z} = -R_{\text{in}} n_i \left(g_n - g_i \right) + g_n \left(\frac{\partial u_n}{\partial z} - \left(v_\parallel - u_n \right) \frac{\partial \ln n_n}{\partial z} \right), \tag{22}$$

We normalize Eqs. (18)-(22) by using Eqs. (6)-(11) and by further defining

$$\tilde{g}_s \doteq g_s v_{\text{th,i}} \sqrt{\pi} \tag{23}$$

and

$$\tilde{u}_s \doteq \frac{u_s}{v_{\text{th,i}}}. \tag{24}$$

In terms of these normalised quantities, Eqs (18)-(22) become

$$\frac{\partial \tilde{g}_i}{\partial \tilde{t}} + \tilde{v}_\parallel \frac{\partial \tilde{g}_i}{\partial \tilde{z}} - \frac{1}{2} \frac{\partial \tilde{\phi}}{\partial \tilde{z}} \frac{\partial \tilde{g}_i}{\partial \tilde{v}_\parallel} = -\tilde{R}_{\text{in}} \tilde{n}_n \left(\tilde{g}_i - \tilde{g}_n \right) + \tilde{g}_i \left(\frac{\partial \tilde{u}_i}{\partial \tilde{z}} - \left(\tilde{v}_\parallel - \tilde{u}_i \right) \frac{\partial \ln \tilde{n}_i}{\partial \tilde{z}} \right), \tag{25}$$

$$\frac{\partial \tilde{g}_n}{\partial \tilde{t}} + \tilde{v}_\parallel \frac{\partial \tilde{g}_n}{\partial \tilde{z}} = -\tilde{R}_{\text{in}} \tilde{n}_i \left(\tilde{g}_n - \tilde{g}_i \right) + \tilde{g}_n \left(\frac{\partial \tilde{u}_n}{\partial \tilde{z}} - \left(\tilde{v}_\parallel - \tilde{u}_n \right) \frac{\partial \ln \tilde{n}_n}{\partial \tilde{z}} \right), \tag{26}$$

$$\frac{\partial \tilde{n}_s}{\partial \tilde{t}} + \frac{\partial \tilde{n}_s \tilde{u}_s}{\partial \tilde{z}} = 0, \tag{27}$$

$$e^{\tilde{\phi}} = \tilde{n}_i, \tag{28}$$

and

$$\tilde{u}_s = \frac{1}{\sqrt{\pi}} \int_{-\infty}^{\infty} d\tilde{v}_\parallel \tilde{g}_n \tilde{v}_\parallel. \tag{29}$$

The above form for the equations is appealing because it maintains the form of an advection equation with the only modification being the addition of source terms. However, it can pose challenges for numerical conservation of quantities such as the 0th velocity moment of g_s. This is because parts of the source terms must cancel upon velocity space integration with some of the advective terms. To ease the task of preserving conservation properties numerically, the equations can be manipulated into the following form in which such cancellations can be built into the discretisation:

$$\frac{\partial \tilde{g}_i}{\partial \tilde{t}} + \frac{\tilde{v}_\parallel}{\tilde{n}_i} \frac{\partial \tilde{n}_i \tilde{g}_i}{\partial \tilde{z}} - \frac{1}{2} \frac{\partial \tilde{\phi}}{\partial \tilde{z}} \frac{\partial \tilde{g}_i}{\partial \tilde{v}_\parallel} = -\tilde{R}_{\text{in}} \tilde{n}_n \left(\tilde{g}_i - \tilde{g}_n \right) + \frac{\tilde{g}_i}{\tilde{n}_i} \frac{\partial \tilde{n}_i \tilde{u}_i}{\partial \tilde{z}}, \tag{30}$$

$$\frac{\partial \tilde{g}_n}{\partial \tilde{t}} + \frac{\tilde{v}_\parallel}{\tilde{n}_n} \frac{\partial \tilde{n}_n \tilde{g}_n}{\partial \tilde{z}} = -\tilde{R}_{\text{in}} \tilde{n}_i \left(\tilde{g}_n - \tilde{g}_i \right) + \frac{\tilde{g}_n}{\tilde{n}_n} \frac{\partial \tilde{n}_n \tilde{u}_n}{\partial \tilde{z}}, \tag{31}$$

$$\frac{\partial \tilde{n}_s}{\partial \tilde{t}} + \frac{\partial \tilde{n}_s \tilde{u}_s}{\partial \tilde{z}} = 0, \tag{32}$$

$$e^{\tilde{\phi}} = \tilde{n}_i, \tag{33}$$

and

$$\tilde{u}_s = \frac{1}{\sqrt{\pi}} \int_{-\infty}^{\infty} d\tilde{v}_\parallel \tilde{g}_n \tilde{v}_\parallel. \tag{34}$$

3. Numerical implementation

The algorithms described in this Section have been implemented in the code, written in the Julia programming language, currently available on GitHub at `https://github.com/mabarnes/moment_kinetics`.

3.1. Time advance

We evolve Eqs. (12)-(15) or Eqs. (30)-(34) using a member of the family of Strong Stability Preserving (SSP) Runge-Kutta (RK) schemes; see, e.g., [3, 4, 5]. Current SSPRK options implemented in the code are SSPRK1 (forward Euler), SSPRK2 (Heun's method) SSPRK3 (Shu-Osher method) and four-stage SSPRK3. The user can also specify the use of 'flip-flop' Lie operator splitting. Operator splitting limits the time advance scheme to second order accuracy in step size, but could be useful for separately

treating different pieces of physics. Here we describe the current default option, which is the four-stage SSPRK3 method without operator splitting.

For convenience of notation, we express the normalised drift kinetic equations for the ions and neutrals in the vector form

$$\frac{\partial \mathbf{f}}{\partial t} = G[\mathbf{f}], \tag{35}$$

with $\mathbf{f}$ the solution vector containing the evolved quantities: $\mathbf{f} = \left(\tilde{f}_i, \tilde{f}_n\right)^T$ if Eqs. (12)-(15) are solved, and $\mathbf{f} = (\tilde{g}_i, \tilde{g}_n, \tilde{n}_i, \tilde{n}_n)^T$ if Eqs. (30)-(34) are solved. The operator G accounts for parallel streaming, parallel acceleration (for the ions) and charge exchange collisions, as well as for the divergence of the particle flux if the density is separately evolved. The four-stage SSPRK3 method for advancing this system of equations is 3rd order accurate in time step size Δt, with a Courant number of two. It is given by

$$
\begin{aligned}
\mathbf{f}^{(1)} &= \frac{1}{2}\mathbf{f}^n + \frac{1}{2}\left(\mathbf{f}^n + \Delta t G\left[\mathbf{f}^n\right]\right), \\
\mathbf{f}^{(2)} &= \frac{1}{2}\mathbf{f}^{(1)} + \frac{1}{2}\left(\mathbf{f}^{(1)} + \Delta t G\left[\mathbf{f}^{(1)}\right]\right), \\
\mathbf{f}^{(3)} &= \frac{2}{3}\mathbf{f}^n + \frac{1}{6}\mathbf{f}^{(2)} + \frac{1}{6}\left(\mathbf{f}^{(2)} + \Delta t G\left[\mathbf{f}^{(2)}\right]\right), \\
\mathbf{f}^{n+1} &= \frac{1}{2}\mathbf{f}^{(3)} + \frac{1}{2}\left(\mathbf{f}^{(3)} + \Delta t G\left[\mathbf{f}^{(3)}\right]\right),
\end{aligned}
\tag{36}
$$

where the superscript n denotes the time level.

We have tested our implementation of SSP RK2 and 4-stage SSP RK3 by calculating the rms error in the distribution function after it is advected in one dimension with constant advection speed $\tilde{v} = 1$ for 10 transits of the domain with length $L = 1$:

$$\epsilon_{\mathrm{rms}} \doteq \sqrt{\frac{1}{N_z}\sum_{j=1}^{N_z}\left|f_i(z_j, t = 10) - f_i(z_j, t = 0)\right|^2}. \tag{37}$$

The results when paired with a finite difference discretisation (third order upwind) are given in Fig. 1. For Chebyshev pseudospectral on a single element with 4-stage SSPRK3, see Fig. 2.

3.2. Spatial discretisation

There are two discretisation schemes implemented in the code: finite differences and Chebyshev (pseudo)spectral elements. The user can choose at run-time which scheme to use for each of the z and $v_\parallel$ coordinates.

3.2.1. Finite difference discretisation.
For the finite difference discretisation, the corresponding coordinate grid is uniform on the domain $[-L/2, L/2]$, with L the coordinate box length. The default method employed for derivatives is 3rd order upwind
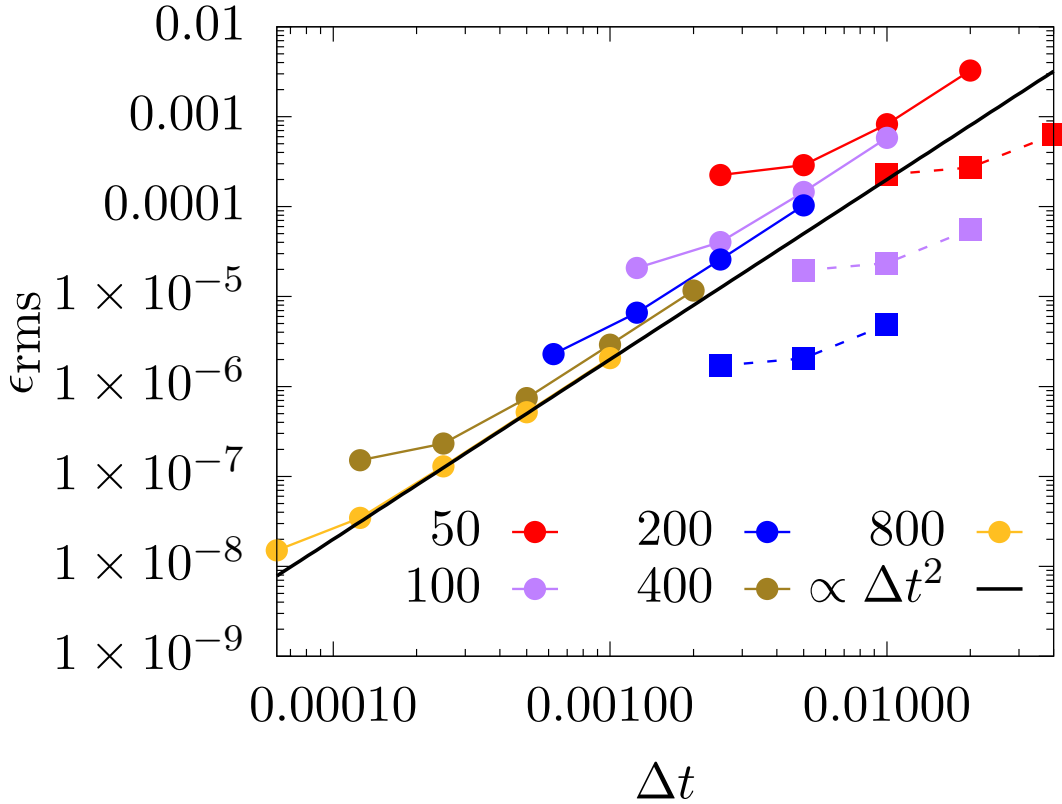
Figure 1. RMS error as a function of time step size Δt and varying values for N_z for both SSP RK2 (solid lines and circles) and for 4-stage SSP RK3 (dashed lines and squares). Due to the CFL restriction that ties temporal resolution to spatial resolution, the range in Δt over which time domain errors dominate is limited for RK2 and is effectively non-existent for RK3.

differences, though 1st and 2nd order schemes are also available as options. For an overview of upwind differences and a discussion of the merits of the different upwind schemes, see, e.g. [6]. The associated integration weights used for field-line averages in z and/or for the $v_\parallel$ integration required for obtaining fields/moments are obtained using the composite Simpson's rule (sometimes referred to as composite Simpson's 1/3 rule):

$$\int_0^L dx\ f(x) \approx \frac{h}{3} \sum_{j=1}^{(N-1)/2} \left(f(x_{2j-1}) + 4f(x_{2j}) + f(x_{2j+1}) \right), \qquad (38)$$

where N is the number of grid points in the coordinate x, and $h = L/(N-1)$ is the uniform grid spacing. The composite rule (38) is only applicable for N odd, so it is supplemented at the boundary by Simpson's 3/8 rule when N is even.

3.2.2. Chebyshev spectral elements. When using Chebyshev spectral elements, the corresponding coordinate grid is the Gauss-Chebyshev-Lobatto grid on each element. For a description of Chebyshev-Gauss quadrature, see, e.g. [7]. Inclusion of the endpoints
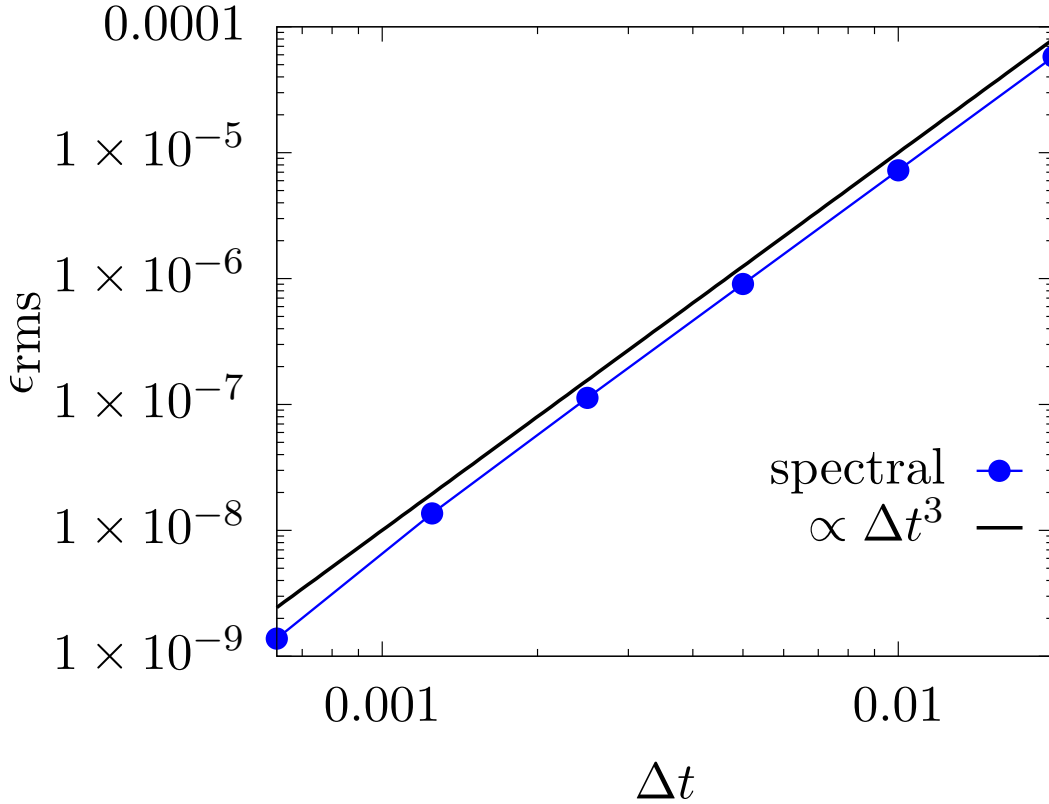
Figure 2. RMS error as a function of time step size Δt for 4-stage SSP RK3 with a Chebyshev pseudospectral discretisation.

within each element facilitates enforcement of continuity at element boundaries, and the use of Chebyshev polynomials as a basis enables the use of Fast Fourier Transforms. In our code, these transforms are done using the widely-used FFTW library [8]. The associated integration weights used for field-line averages in z and/or for the $v_\parallel$ integration required for obtaining fields/moments are obtained using Clenshaw-Curtis quadrature rules [9]. Clenshaw-Curtis quadrature is convenient, as it allows for the use of endpoints in the integration domain (which is dictated by the use of a Gauss-Chebyshev-Lobatto grid) while still exactly integrating polynomials up to degree $N-1$, with N the number of points within the element.

A 1D advection test demonstrating the spectral accuracy of the Chebyshev scheme on a single element is given in Fig. 3, where the rms error is given by Eq. (37). The maximum stable time step subject to the CFL restriction is plotted as a function of the number of z grid points on a single element in Fig. 4 and as a function of the number of elements N_{elem} with $N_z = 9$ fixed in Fig. 5. Slight deviations from the expected scalings are likely due to the numerical dissipation that is introduced by the use of the derivative from the upwind element at the overlapping point at element boundaries and at the boundary of the periodic domain.
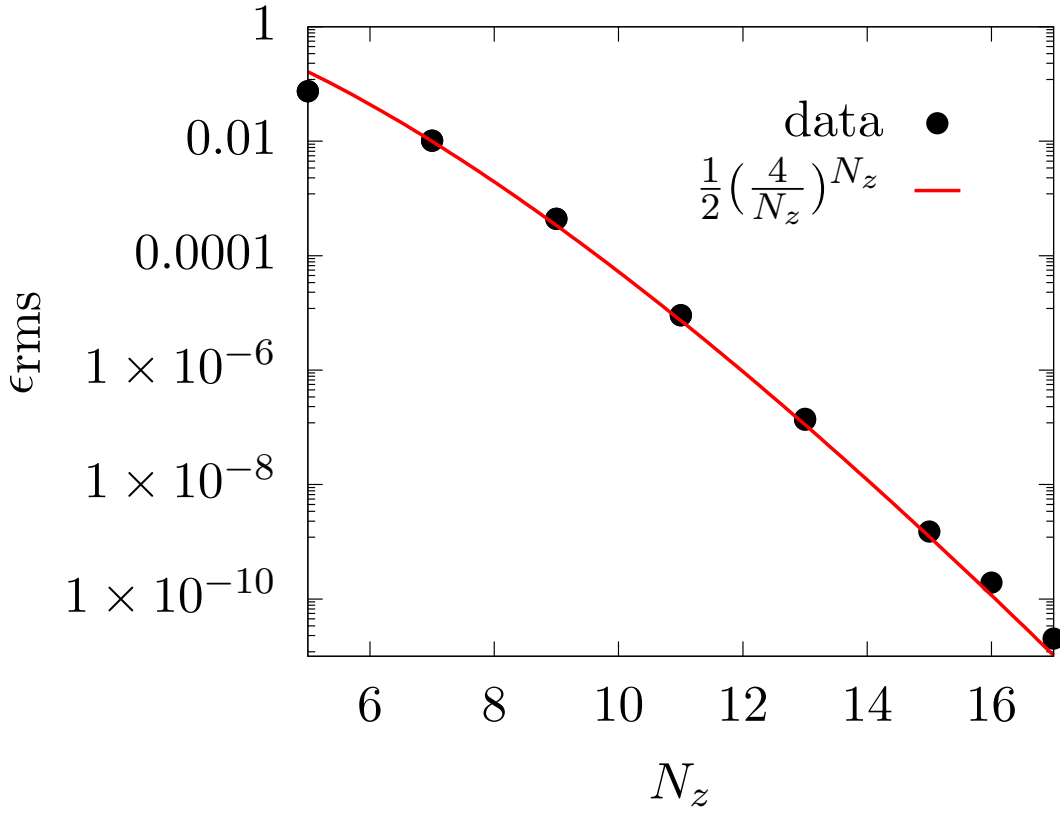
Figure 3. RMS error as a function of the number of grid points N_z. The time advance scheme used is 4-stage SSP RK3.

3.3. conservation properties

The field-line-averaged density, $\int dz \ n$, should be conserved, as should $\int dv_{\parallel} g = 1$. We consider two approaches to ensuring that these properties are preserved by the numerical scheme: carefully chosen discretisation of the equations in conservative form and conserving corrections applied at the end of each time level.

3.3.1. conservative differencing To conserve particle number, the discretisation must satisfy

$$0 = \sum_{j=1}^{N_{\text{elem}}} \frac{\partial}{\partial t} \int_{\Omega_j} dz^j \ n^j = -\int_{\Omega_j} dz^j \frac{\partial \Gamma^j}{\partial z^j}$$

$$= -\sum_{j=1}^{N_{\text{elem}}} \sum_{k=1}^{N_z} w_k^j \left(\frac{\partial \Gamma^j}{\partial z^j} \right)_k,$$

(39)

where $\Gamma = nu$ is the particle flux, N_{elem} is the number of elements, N_z is the number of grid points per element, Ω_j is the domain in z corresponding to the jth element, the superscript j denotes evaluation on the jth element, and w_k^j is the integration weight
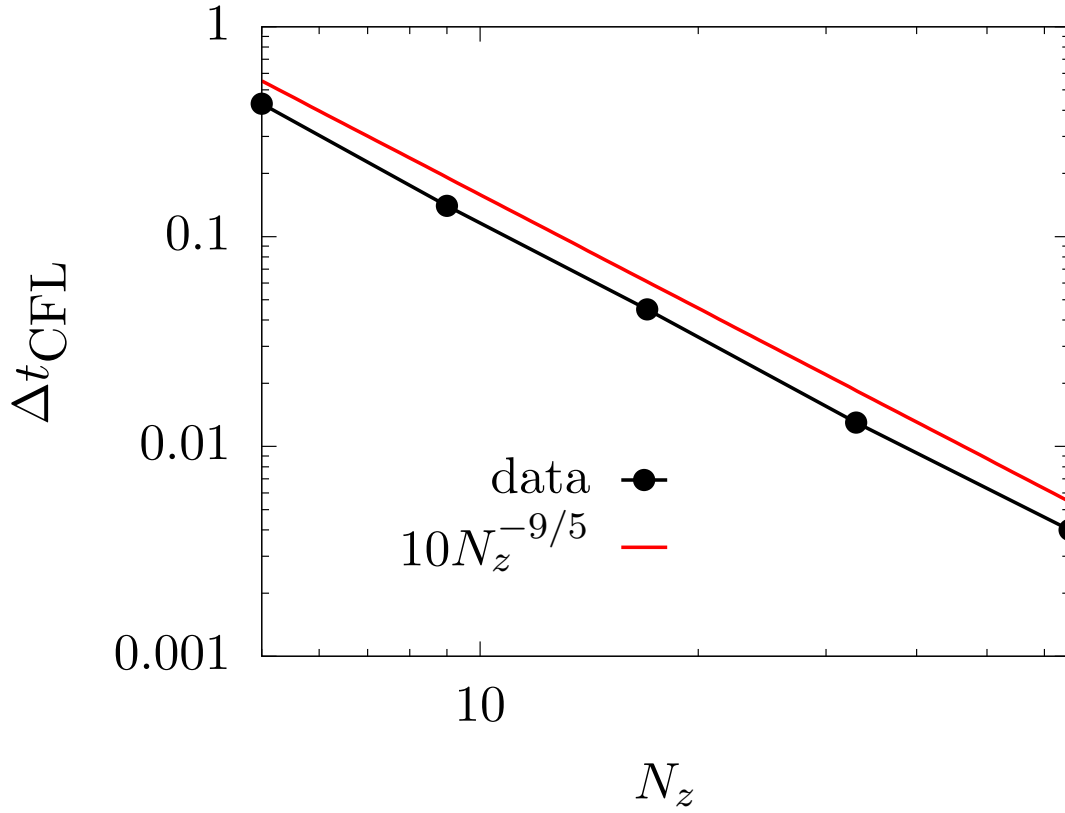
Figure 4. Maximum stable time step subject to the CFL restriction as a function of the number of Gauss-Chebyshev-Lobatto grid points. The max stable time step scales a bit more weakly than $1/N_z^2$, as expected.

associated with the kth grid point within the jth element. For expression (39) to be satisfied, there are three requirements that must be met. First, the contributions to the integral from interior points on each element must cancel with one another. This requires a centred difference scheme if finite differences are used. As shown in Appendix A, it is automatically satisfied if the flux derivative is obtained using the Chebyshev pseudo-spectral method, and the integral is computed using Clenshaw-Curtis quadrature. Second, the fluxes must be continuous across element boundaries. For this to be guaranteed, the derivative of the flux itself must be single-valued at the element boundaries. This forces one to choose the flux derivative at the boundary between elements to be the average of the flux derivatives on each element. Finally, the fluxes must vanish or cancel one another at the boundaries of the simulation domain. This forces one to use either zero boundary conditions or to again use the average of the flux derivatives on each element with the assumption of periodicity.

Next we consider how to ensure $\int dv_\| g = 1$. The terms involving z derivatives of g on each side of the drift kinetic equation will cancel as long as the differencing is done consistently for each term, as well as using g and u at the same time level. The charge exchange term should also vanish as long as g_i and g_n are used at the same time
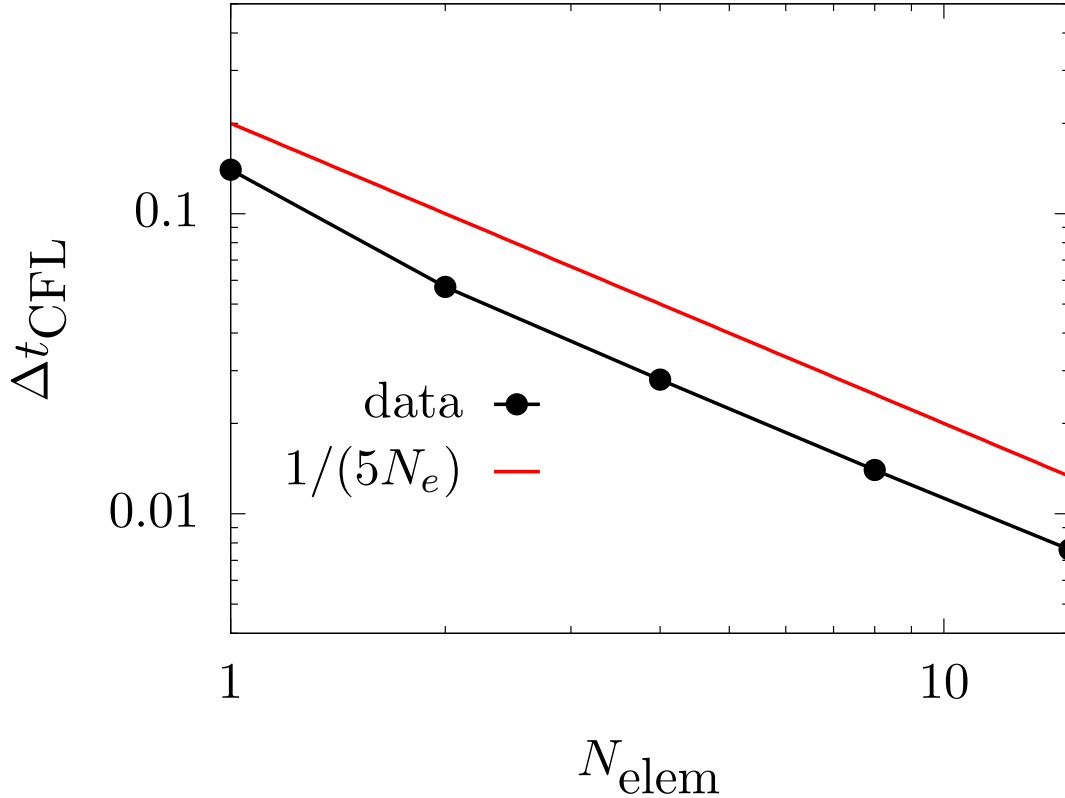
Figure 5. Maximum stable time step subject to the CFL restriction as a function of the number of elements with the number of grid points per element fixed at 9. The minimum grid spacing scales inversely with the number of elements, leading to a max stable time step that is inversely proportional to the number of elements N_{elem}.

level. The only non-trivial term then is the parallel acceleration. For this term to vanish upon $v_\parallel$ integration, the fundamental theorem of calculus must hold numerically; i.e., $\int dv_\parallel (\partial g / \partial v_\parallel) = g(v_{\parallel,\mathrm{max}}) - g(v_{\parallel,\mathrm{min}}) = 0$, where $v_{\parallel,\mathrm{max}}$ and $v_{\parallel,\mathrm{min}}$ are the maximum and minimum values of $v_\parallel$ included in the grid. For the last equality, the values of g at the boundaries in $v_\parallel$ must be the same. This could be achieved either with periodic BCs or with zero BCs. However, there is the complication that the drift kinetic equation drives non-periodic solutions that only decay to zero at $v_\parallel \to \pm\infty$. To enforce periodicity without modifying $\int dv_\parallel g$, we set the boundary values to be the average of the nominal values at the endpoints in $v_\parallel$.

Taken together, these requirements remove the possibility of using numerical dissipation via, e.g., upwind differencing or upwind fluxes at element boundaries, to improve numerical stability. This is problematic for advection-dominated problems like the one we are considering, as in the absence of some form of numerical dissipation the scheme is unstable.

3.3.2. conserving corrections   The second approach to ensuring numerically the desired conservation properties is to correct the numerical solutions for n and g at the end of each time step. For the density, one can set

$$n^{m+1} = \hat{n}^{m+1} + n^m \left(1 - \frac{\int dz \; \hat{n}^{m+1}}{\int dz \; n^m} \right), \tag{40}$$

where $\hat{n}^{m+1}$ is the updated solution (at time level $m+1$) to the continuity equation before applying any conserving correction. This guarantees that $\int dz \, (n^{m+1} - n^m) = 0$. Note that the superscripts here refer to the time level, not the element index. The additional error in the density introduced by this correction is

$$
\begin{aligned}
n^m \left(1 - \frac{\int dz \; \hat{n}^{m+1}}{\int dz \; n^m} \right) &= n^m \left(1 - \frac{\int dz \; \left(n_{\text{exact}}^{m+1} + \epsilon^m \right)}{\int dz \; n^m} \right) \\
&= n^m \frac{\int dz \; \epsilon^m}{\int dz \; n^m} = \mathcal{O}(\epsilon^m),
\end{aligned}
\tag{41}
$$

where ϵ^m is the error due to numerical discretisation, and n_{exact}^{m+1} is the solution for $\hat{n}^{m+1}$ in the limit $\epsilon^m = 0$.

A similar technique can be applied to conserve $\int dv_\parallel g$. In particular, we set

$$g^{m+1} = \hat{g}^{m+1} + g^m \left(1 - \int dv_\parallel \hat{g}^{m+1} \right), \tag{42}$$

where $\hat{g}^{m+1}$ is the updated solution to the drift kinetic equation before applying any conserving correction. This ensures $\int dv_\parallel g^{m+1} = 1$, provided $\int dv_\parallel g^m = 1$. Again, the additional error in g associated with this correction is $\mathcal{O}(\delta^m)$, where δ^m is the discretisation error.

This approach is simple, does not change the order of accuracy of the discretisation scheme and allows for the use of numerical dissipation to improve numerical stability properties. Results showing its efficacy are given in Sec. 4

4. Numerical results

To benchmark our numerical implementation of the moment-based approach encapsulated in Eqs. (30)-(34), we compare our simulation results with the analytical benchmarks developed in [2] and with the numerical results obtained by directly solving the kinetic system corresponding to Eqs. (12)-(15). The results reported here were obtained using the conservative differencing detailed in Sec. 3.3.1 for the continuity equation and for the source terms, while the conserving correction given by Eq. 42 is applied to ensure that $\int dv_\parallel g_s = 1$.

We have initialised the distribution functions for the ions and neutrals to be of the form

$$\tilde{g}_s = \left(\frac{T_e}{\overline{T}_s} \right)^{1/2} \exp \left(-\tilde{v}_\parallel^2 \frac{T_e}{\overline{T}_s} \right), \tag{43}$$

with $n_s = \overline{n}_s + \delta n_s$ and $T_s = \overline{T}_s + \delta T_s$, and an overline denoting a field line average. The piece of the density that varies along z, δn_s, is chosen to be small compared to $\overline{n}_s$ ($\delta n_s / \overline{n}_s = 0.001$) so that the system of equations can be linearised to a good approximation. This facilitates comparisons with the linear analytical theory presented in [2]. For all cases shown here, $\overline{n}_i = \overline{n}_n = N_e/2$, $\overline{T}_i = \overline{T}_n = T_e$ and $m_i = m_n$. The charge exchange collision frequency is varied, and damping rates and frequencies are extracted by considering the time evolution of the spatially-varying component of the electrostatic potential, $\delta\phi$. In particular, a least-squares fit for $\delta\phi(t)/\delta\phi(t_0)$ is done for each simulation to a function of the form $\exp(-\gamma(t - t_0))\cos(\omega t - \varphi)/\cos(\omega t_0 - \varphi)$ to obtain the damping rate γ, frequency ω and phase φ. The results are given in Fig. 6. There is good agreement across a wide range of charge exchange collision frequencies, both for the damping of finite frequency modes (corresponding to the solid lines) and to a zero frequency mode that appears at larger collisionalities (dashed-dotted lines). The minor discrepancy between the analytical and numerical damping rates that is apparent for the case with normalised charge exchange collision frequency near 0.7 is due to the simultaneous presence of both modes with similar damping rates.
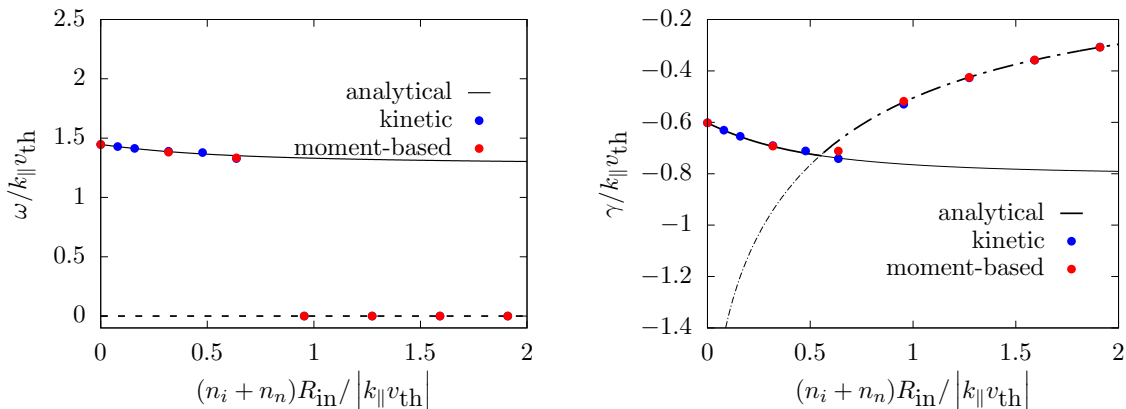

Figure 6. Normalized damping rate and real frequency as a function of the charge exchange collision frequency. Note that the normalising v_{th} employed here differs from the $v_{\text{th,i}}$ employed in the text: It is chosen to be $v_{\text{th}} = \sqrt{2T_i/m_i}$ to facilitate comparison with the analytical results obtained in [2].

In Figure 7 we show the difference in conservation properties between cases for which the mixed conservative differencing and conservative corrections indicated at the beginning of the Section are employed and those for which no conserving correction is applied. With the conservative implementation, both the particle number and $\int dv_{\parallel} g$ are conserved to machine precision, regardless of numerical resolution.

5. Future plans

Now that we have a proof-of-concept implementation of the moment-based approach to solving the 1+1D kinetic problem, we plan to extend the treatment to include separate
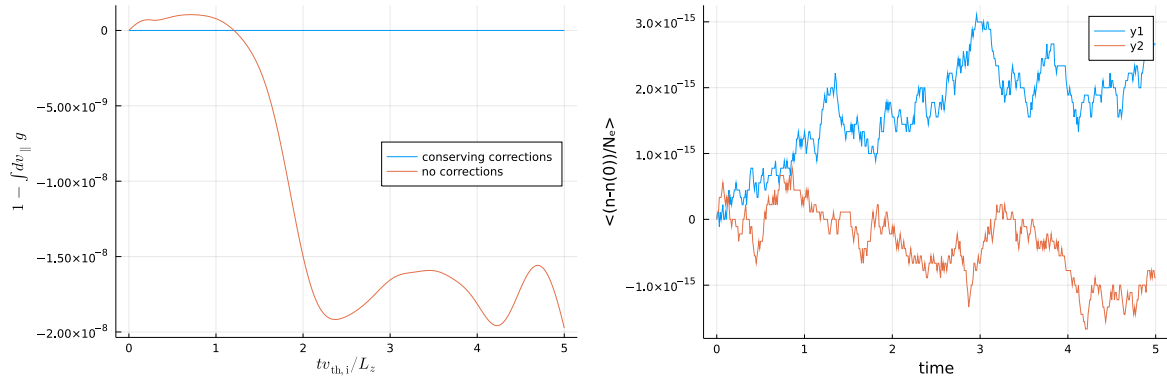
Figure 7. Time evolutions of the conservation error for $\int dv_\parallel g$ (left) and for the particle number (right). The velocity moment of g is guaranteed to be unity in the blue case because the conserving corrections described in Sec. 3.3 are applied. Conservative differencing in the continuity equation and the use of average fluxes at element boundaries ensures particle conservation for both simulations. Both simulations were run for $\overline{T}_i = \overline{T}_n = T_e$, normalised $R_{\rm in} \approx 0.3$ and used very low resolution to enhance the non-conservation: a Chebyshev pseudo-spectral discretisation was used with $N_z = 5$ on one element and $N_v = 9$ on five elements.

evolution of the parallel flow and parallel pressure. Inclusion of a separately evolved parallel flow should enable us to include kinetic electrons in our model and test various numerical approaches to obtaining the electrostatic potential in an efficient way.

Appendix A. Conservative differencing of the continuity equation

We start with the continuity equation,

$$\frac{\partial n}{\partial t} + \frac{\partial \Gamma}{\partial z} = 0, \tag{A.1}$$

and we expand the particle flux Γ in Chebyshev polynomials on each of $N_{\rm elem}$ elements so that

$$\Gamma_i^j \doteq \sum_{n=0}^{N-1} \hat{\Gamma}_n^j T_n(z_i) \tag{A.2}$$

is the particle flux at the ith grid point within the jth element, and $T_n(z_i)$ is a Chebyshev polynomial of the first kind. The derivative appearing in the continuity equation is then

$$\frac{\partial \Gamma^j}{\partial z} = \sum_{n=0}^{N-1} \hat{\Gamma}_n^j \frac{\partial T_n(z)}{\partial z} = \sum_{n=0}^{N-2} d_n^j T_n(z), \tag{A.3}$$

with d_n^j related to $\hat{\Gamma}_n^j$ via

$$d_{n-1}^j = \frac{1}{c_{n-1}} \left(2n\hat{\Gamma}_n^j + d_{n+1}^j \right), \tag{A.4}$$

where $d_{N-1}^j = d_N^j = 0$ and $c_n = 2$ if $n = 0$ and $c_n = 1$ for $n > 0$.

The field-line-averaged density should be conserved according to the continuity equation. This can be achieved by carefully choosing the discretisation to be of a conservative form. In particular, the discretisation must satisfy

$$
\begin{aligned}
0 = \frac{\partial}{\partial t} \int_{\Omega_j} dz \; n &= -\int_{\Omega_j} dz^j \frac{\partial \Gamma^j}{\partial z^j} \\
&= -\sum_{i=1}^{N_z} w_i^j \left(\frac{\partial \Gamma^j}{\partial z^j} \right)_i \\
&= \Gamma_{N_z}^j - \Gamma_1^j,
\end{aligned}
\tag{A.5}
$$

where the integration weights are given by the set $\{w_i^h\}$, and the equality in the last line holds as long as the integration scheme is chosen to exactly integrate polynomials of degree less than $N_z - 1$. The Clenshaw-Curtis quadrature satisfies this requirement.

However, there is one more issue to consider: continuity of the density across element boundaries. If we enforce continuity, the derivative of the flux must be single-valued at the element boundaries. Let the flux derivative at the element boundaries be

$$
\frac{\partial \Gamma_b^j}{\partial z^j} = \alpha \frac{\partial \Gamma_{N_z}^j}{\partial z^j} + (1 - \alpha) \frac{\partial \Gamma_1^{j+1}}{\partial z^{j+1}},
\tag{A.6}
$$

with $\alpha \in [0, 1]$.

The time rate of change of the field-line-averaged density is thus

$$
\begin{aligned}
\frac{\partial}{\partial t} \int dz \; n = \sum_{j=1}^{N_e} \int_{\Omega_j} dz^j n^j &= \sum_{j=1}^{N_e} \left(\Gamma_{N_z}^j - \Gamma_1^j \right) \\
&+ \sum_{j=1}^{N_e - 1} \left(\left(w_{N_z}^j + w_1^{j+1} \right) \frac{\partial \Gamma_b^j}{\partial z^j} - w_{N_z}^j \frac{\partial \Gamma_{N_z}^j}{\partial z^j} - w_1^{j+1} \frac{\partial \Gamma_1^{j+1}}{\partial z^{j+1}} \right).
\end{aligned}
\tag{A.7}
$$

Because Γ is single-valued at element boundaries, each of the interior terms in the first sum on the RHS above cancel, leaving only the contribution from $j = 1$ and $j = N_{\text{elem}}$. The final sum is then the deviation from exact particle conservation. This can be made to vanish by choosing α in Eq. (A.6) to be

$$
\alpha = \frac{w_{N_z}^j}{w_{N_z}^j + w_1^{j+1}},
\tag{A.8}
$$

which evaluates to $1/2$ if the grids are identical in neighbouring elements. The same treatment must also be applied at the exterior boundaries to ensure exact numerical conservation. Note that this is possible with periodic BCs but not with a zero BC.

[1] M. Barnes, F. I. Parra, and M. R. Hardman. Numerical study of 1d drift kinetic models with periodic boundary conditions. *Excalibur/Neptune Report*, 2:2047357–TN–01–02 M2.1, 2021.

[2] F. I. Parra, M. Barnes, and M. R. Hardman. 1d drift kinetic models with periodic boundary conditions. *Excalibur/Neptune Report*, 1:2047357–TN–01–02 M1.1, 2021.

[3] C.-W. Shu and S. Osher. Efficient implementation of essentially non-oscillator shock-capturing schemes. *J. Comp. Phys.*, 77:439–471, 1988.

[4] S. Gottlieb and C.-W. Shu. Total variation diminishing runge-kutta methods. *Mathematics of Computation*, 67:73–85, 1998.

[5] S. Gottlieb, C.-W. Shu, and E. Tadmor. Strong stability-preserving high-order time discretization methods. *SIAM Rev.*, 43:89, 2001.

[6] D. R. Durran. *Numerical methods for wave equations in geophysical fluid dynamics*. Springer, 1999.

[7] M. Abramowitz and I. A. Stegun. *Handbook of Mathematical Functions with Formulas, Graphs, and Mathematical Tables*. Dover, New York, 1972.

[8] Matteo Frigo and Steven G. Johnson. The design and implementation of FFTW3. *Proceedings of the IEEE*, 93(2):216–231, 2005. Special issue on "Program Generation, Optimization, and Platform Adaptation".

[9] C. W. Clenshaw and A. R Curtis. A method for numerical integration on an automatic computer. *Numerische Mathematik*, 2:197, 1960.